PNNL-35345

Magnetic Nanoparticle Extraction of Lithium from Produced Waters (CRADA 483)

Final Project Report

November 2023

Sun Hae Ra Shin
Praveen K. Thallapally

Prepared for the U.S. Department of Energy
under Contract DE-AC05-76RL01830

NOTICE

This report was produced by Battelle Memorial Institute under Contract No. DE-AC05-76RL01830 with the Department of Energy. During the period of commercialization or such other time period specified by the Department of Energy, the Government is granted for itself and others acting on its behalf a nonexclusive, paid-up, irrevocable worldwide license in this data to reproduce, prepare derivative works, and perform publicly and display publicly, by or on behalf of the Government. Subsequent to that period, the Government is granted for itself and others acting on its behalf a nonexclusive, paid-up, irrevocable worldwide license in this data to reproduce, prepare derivative works, distribute copies to the public, perform publicly and display publicly, and to permit others to do so. The specific term of the license can be identified by inquiry made to the Contractor or DOE. NEITHER THE UNITED STATES NOR THE UNITED STATES DEPARTMENT OF ENERGY, NOR ANY OF THEIR EMPLOYEES, MAKES ANY WARRANTY, EXPRESS OR IMPLIED, OR ASSUMES ANY LEGAL LIABILITY OR RESPONSIBILITY FOR THE ACCURACY, COMPLETENESS, OR USEFULNESS OF ANY DATA, APPARATUS, PRODUCT, OR PROCESS DISCLOSED, OR REPRESENTS THAT ITS USE WOULD NOT INFRINGE PRIVATELY OWNED RIGHTS.

Printed in the United States of America

Available to DOE and DOE contractors from the Office of Scientific and Technical Information, P.O. Box 62, Oak Ridge, TN 37831-0062
www.osti.gov
ph: (865) 576-8401
fox: (865) 576-5728
email: reports@osti.gov

Available to the public from the National Technical Information Service
5301 Shawnee Rd., Alexandria, VA 22312 ph: (800) 553-NTIS (6847)
or (703) 605-6000
email: info@ntis.gov
Online ordering: http://www.ntis.gov

PNNL-35345

Magnetic Nanoparticle Extraction of Lithium from Produced Waters (CRADA 483)

Final Project Report

November 2023

Sun Hae Ra Shin
Praveen K. Thallapally

Prepared for
the U.S. Department of Energy
under Contract DE-AC05-76RL01830

Pacific Northwest National Laboratory
Richland, Washington 99354

Summary

The demand for lithium in the energy production industry is expected to increase sharply, development of simple and cost-effective techniques for lithium production and recovery from various lithium sources is essential. In this project, core/shell magnetic nanoparticles were successfully designed to selectively extract lithium from aqueous lithium sources as an extension of Pacific Northwest National Laboratory's magnetic nanofluid extraction technology. The core/shell magnetic nanoparticles are composed of manganese oxide-based lithium ion-sieve shells, which allow selective lithium uptake from brines with multiple coexisting ions, over iron oxide cores, which can respond to external magnetic fields for effective recovery and reuse of adsorbents from a liquid. The synthesized lithium ion-sieves and core/shell magnetic nanoparticles were characterized using several techniques to reveal their crystallinity and morphology. The lithium uptake properties of the lithium ion-sieves and core/shell magnetic nanoparticles were evaluated in terms of lithium adsorption capacity, removal percentage, selectivity, and cycling performance in simulated and natural brines. Magnetic properties of the core/shell magnetic nanoparticles were tested by measuring magnetic saturation, and magnetic response of colloidal solutions containing the core/shell magnetic nanoparticles was tested with permanent magnets.

No subject inventions were generated under this CRADA.

Acknowledgments

We thank Mr. Jerry Mills, and Mr. Bart Mills at Moselle Technologies for their support.

Acronyms and Abbreviations

HMnO	hydrogen manganese oxide(s)
HTO	hydrogen titanium oxide(s)
LMnO	lithium manganese oxide(s)
PNNL	Pacific Northwest National Laboratory
PXRD	powder x-ray diffraction
TEM	transmission electron microscopy

Contents

Figures

Tables

1.0 Introduction

Lithium (Li) is one of the most important materials in the energy production industry. Li has been widely used in electric vehicles and portable electronics such as laptops and cell phones. Because demand for Li is expected to grow rapidly, Li production and recovery techniques are essential and must be significantly enhanced in quality and yield of product. While Li is present over a wide range of locations and concentrations in the U.S., as shown in Figure 1 (Kumar et al. 2019), Li extraction techniques from aqueous Li resources such as geothermal brines and produced waters have advantages over extraction techniques from ores because they are environmentally friendly and cost-effective.

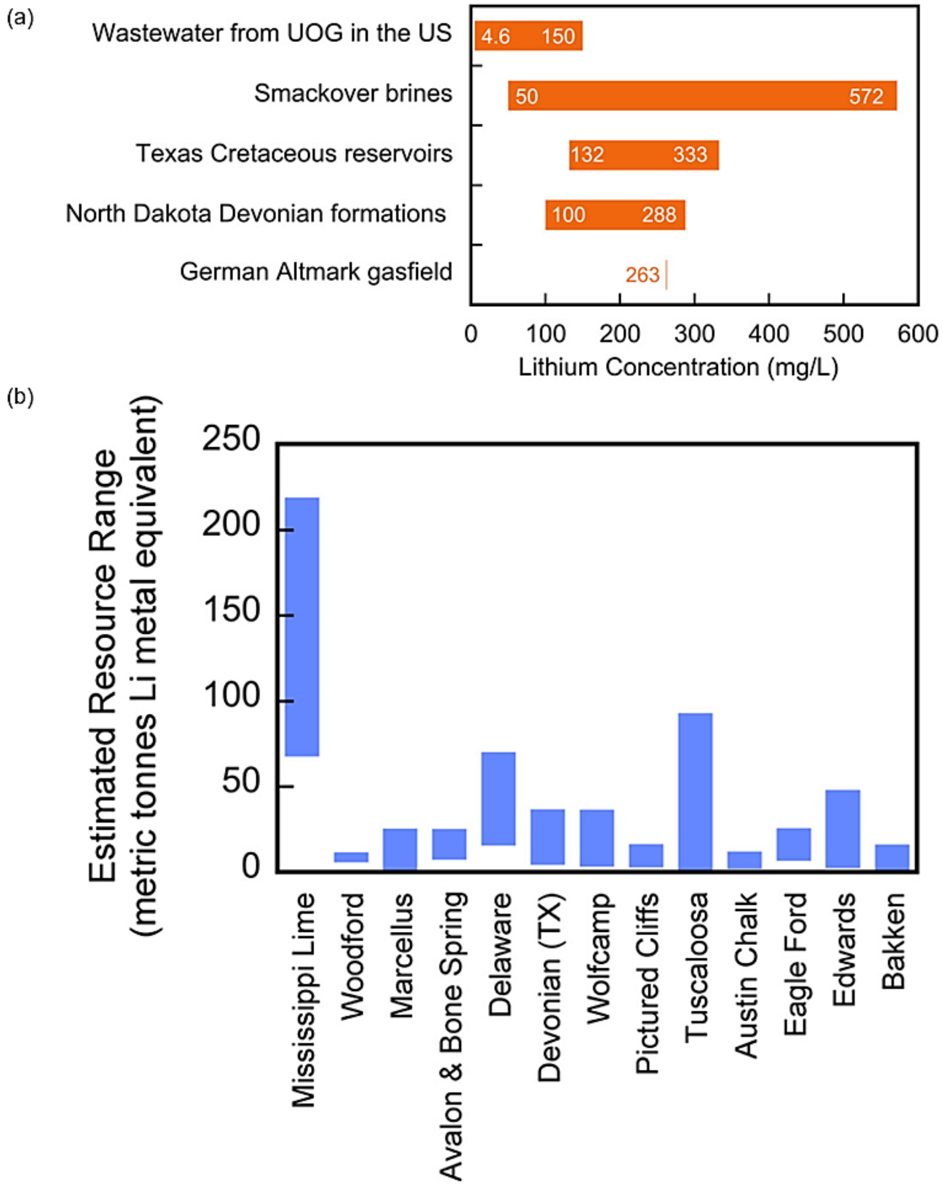

Figure 1. (a) Li concentration in water from unconventional oil and gas (UOG) fields in the U.S. and some oil field brines. (b) Estimated resource range in metric tons of Li metal equivalent in wastewater from UOG resources in the U.S. (Kumar et al. 2019)

Current technique to produce Li from brines relies largely on a solar evaporation and precipitation method (Kumar et al. 2019), which is effective but is time-consuming and geographically constrained, and requires high Li concentration (>500 mg/L). Recently, several techniques have been developed to reduce processing time and obtain high-purity Li product from low-Li-concentration resources. For example, Li can be extracted from an aqueous phase by using a solvent extraction. This solvent extraction method is more selective for Li over other monovalent ions but entails pretreatment steps to remove divalent ions and organic impurities from brines. A membrane process can be applied to Li separation from brine where Li concentration is low. Like other membrane applications, the membrane-based method requires temperature and pressure controls, and fouling can be a significant concern. Lithium can be precipitated by adding chemicals such as phosphoric acid. Because Li phosphate is poorly soluble in aqueous solution, the phosphate precipitation method can shorten processing time compared to the conventional carbonate precipitation method. When Li is desired in the form of Li carbonate or hydroxide, additional conversion steps are required. Adsorption using strong acid cation-exchange resin has been recognized as an effective method to recover cations from solution. However, typical ion-exchange resins are not practical for use in Li extraction because Li has lower affinity for the ion-exchange resins than other cations, which leads to low selectivity for Li over other cations.

Li ion-sieves have become known as the most effective adsorbent materials; their unique chemical structures can selectively recover Li from brines (Xu et al. 2016). The common Li ion-sieves are based on aluminum hydroxide, lithium manganese oxide (LMnO), and lithium titanium oxide, because lithium can be adsorbed into or can easily penetrate their crystalline metal oxide structures. Although Li ion-sieves exhibit superior Li capacity and selectivity, these powdered adsorbents cannot be used directly in aqueous Li resources because they are difficult to handle and to recover from a liquid after Li uptake. However, separation using magnetic particles can be a simple, effective method for separating particles from a liquid, as shown from Pacific Northwest National Laboratory's (PNNL)'s magnetic nanofluid extraction technology for extracting rare earth elements from brines (Figure 2) (Elsaidi et al. 2018; Liu et al. 2021).

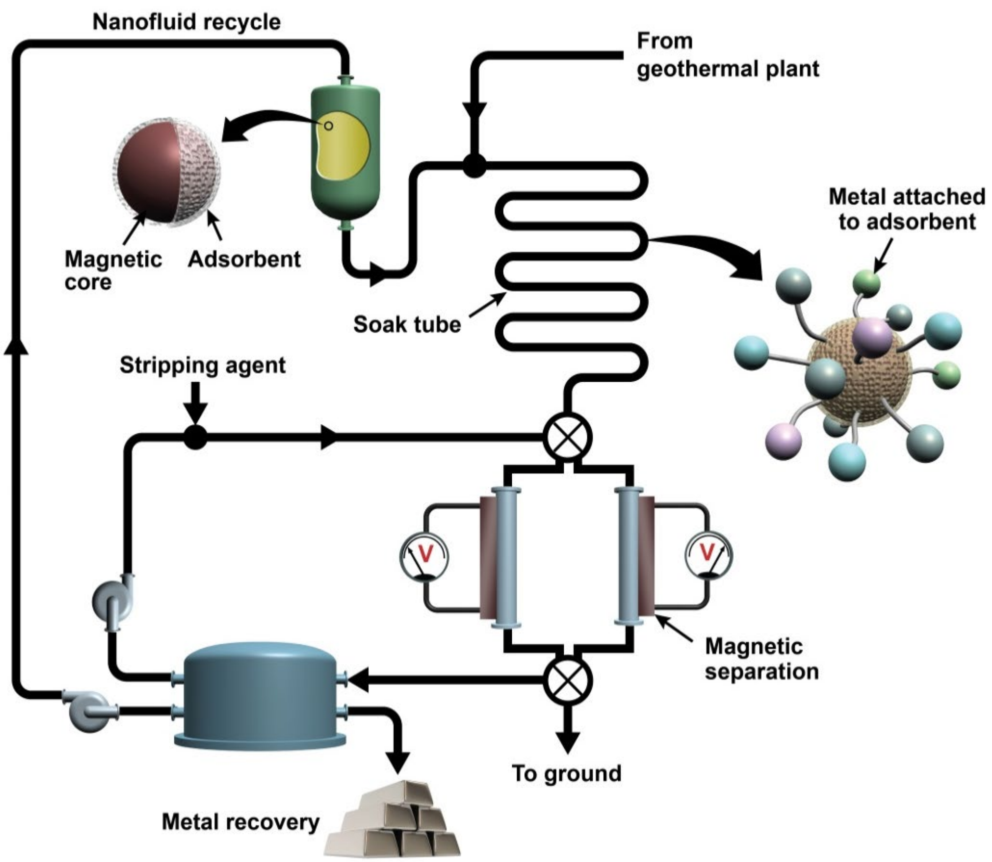

Figure 2. Schematic diagram of magnetic nanofluid extraction system

Therefore, PNNL proposes to extend magnetic separation technology to extracting Li from brines by designing core/shell magnetic nanoparticles that are composed of Li ion-sieve shells enveloping magnetic cores for selective Li uptake from brines that contain multiple coexisting ions for efficient recovery of the adsorbents from a liquid and subsequent reuse.

2.0 Hydrogen Manganese Oxides as Lithium Ion-Sieves

2.1 Synthesis of Hydrogen Manganese Oxides

The shell component of the core/shell structure used in this work is ion-sieves of hydrogen manganese oxide (HMnO), which exchanges H for Li under appropriate conditions.

Hydrogen manganese oxides (HMnO) were synthesized as Li ion-sieves in three steps. In the first step, manganese dioxide (MnO_2) was prepared by mixing manganese sulfate and ammonium persulfate in deionized water (Wang and Li 2003). The solution was placed in a Teflon-lined, stainless-steel autoclave and heated at 140°C for 12 h. The powder x-ray diffraction (PXRD) pattern of the MnO_2 (Figure 3) shows diffraction peaks with 2θ at 28.7°, 37.5°, 40.9°, 42.8°, 46.1°, 56.7°, 59.3°, and 65.0°, which can be indexed to the (110), (101), (200), (111), (210), (211), (220), and (002) planes of β-MnO_2, respectively.

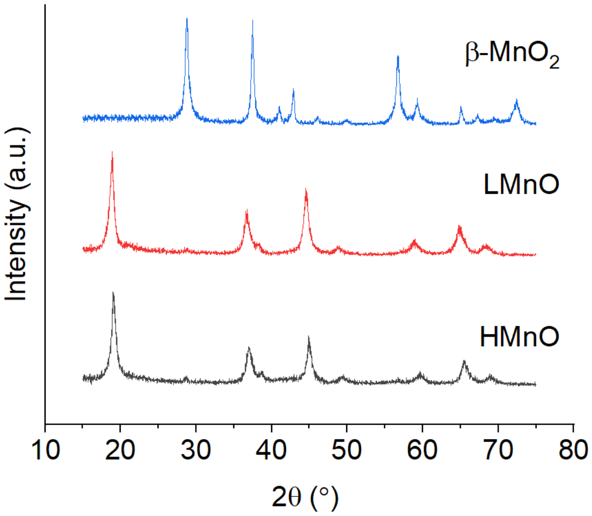

Figure 3. PXRD patterns of β-MnO_2, LMnO, and HMnO

Next, the MnO_2 powder was impregnated with an equimolar amount of lithium nitrate solution to produce LMnO (Zandevakili et al. 2014). After the product was dried overnight in an oven at 100°C, it was calcined at 450°C for 48 h. The PXRD pattern of the LMnO (Figure 3) shows diffraction peaks with 2θ at 18.9°, 36.8°, 44.5°, 49.0°, 58.9°, 64.8°, and 68.3°, which can be indexed to the (111), (311), (400), (331), (511), (440), and (531) planes, respectively, of $Li_{1.6}Mn_{1.6}O_4$.

In the third step, the LMnO was converted to HMnO by dispersing it in a solution of hydrochloric acid (HCl) and manganese chloride ($MnCl_2$) overnight. The PXRD pattern of the resulting HMnO was identical to that of the LMnO (Figure 3), suggesting that the HMnO structure was retained when the Li in LMnO was replaced by H during acid treatment.

To study the kinetics of Li exchange, the LMnO was stirred in 0.1 M HCl (1 mg/mL) at room temperature and the Li concentration in the supernatant solution was measured using inductively coupled plasma optical emission spectroscopy (ICP-OES). The Li exchange rate was calculated as follows:

$$Li\ exchange\ (\%) = \frac{C_{Li} \times V}{m_{LMnO} \times \omega_{Li}} \times 100 \tag{1}$$

where C_{Li} = the concentration of Li in the solution (mg/L)
V = the solution volume (L)
m_{LMnO} = the mass of LMnO (g)
ω_{Li} = the mass fraction of Li in LMnO (%)

Figure 4a shows that 90% of Li was exchanged within 2 h and nearly complete Li exchange (ca. 95% or higher) was achieved after 18 h.

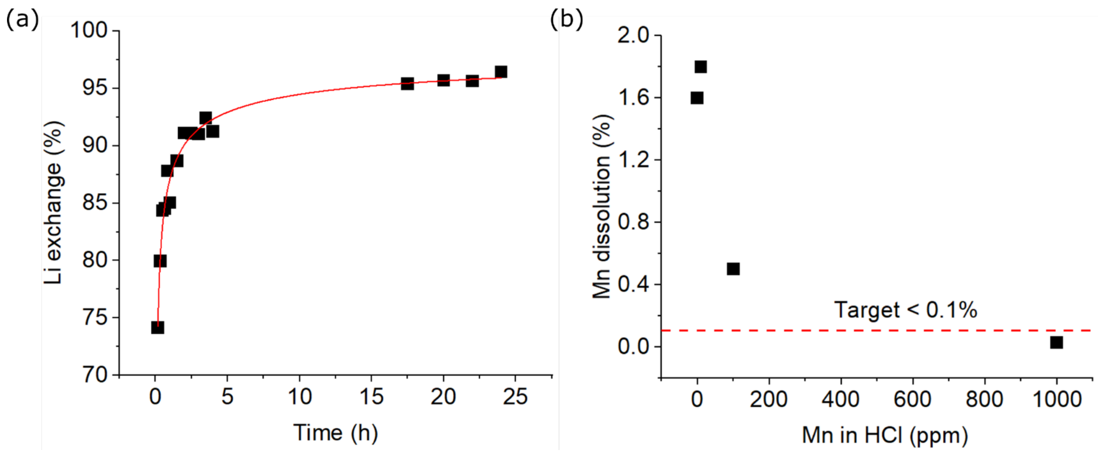

Figure 4. (a) Kinetics of Li exchange in LMnO and (b) loss of Mn into the solution from LMnO during Li exchange in acidic solution

Leaching of Mn from the LMnO could lead to destruction of the LMnO structure during acid treatment; to explore how to mitigate this, the effect of Mn concentration in acidic solution on Mn leaching was investigated (Figure 4b). The LMnO was stirred in HCl solution containing Mn concentrations of 0–1000 ppm, and then Mn concentration in the supernatant solution was analyzed using ICP-OES. The loss of Mn into solution was calculated as follows:

$$Mn\ dissolution\ (\%) = \frac{C_{Mn} \times V}{m_{LMnO} \times \omega_{Mn}} \times 100 \qquad (2)$$

where C_{Mn} = the concentration of Mn in the solution (mg/L)
ω_{Mn} = the mass fraction of Mn in LMnO (%)

The dissolution loss of Mn decreased from 1.6% to 0.03% as Mn concentration in the HCl solution increased from 0 to 1,000 ppm; 0.03% is lower than our target value of Mn loss 0.1%.

2.2 Lithium Extraction from Brines by HMnO

The Li adsorption kinetics of HMnO was studied by stirring HMnO into lithium carbonate (Li_2CO_3) solution (Li 100 ppm) at three pH levels (pH was adjusted by adding HCl) at room temperature. The concentration of HMnO in these brines was 1 mg/mL. As shown in Figure 5, the Li concentration in the brines decreased rapidly—within 5 h—indicating fast Li uptake by HMnO, and then gradually decreased as it approached equilibrium. To estimate the Li uptake, Li adsorption capacity (Q) was calculated using Equation (3), and the adsorption kinetics data were modelled with the pseudo-second-order kinetics equation, Equation (4) (Ünlü and Ersoz 2007):

$$Q = \frac{(C_{Li,0} - C_{Li}) \cdot V}{m_{HMnO}} \qquad (3)$$

where Q = the Li adsorption capacity (mg/g)
$C_{Li,0}$ = the initial concentration of Li in the solution (mg/L)
mHMnO = the mass of HMnO (g)
V = volume of brine.

$$\frac{t}{Q_t} = \frac{1}{kQ_e^2} + \frac{t}{Q_e} \tag{4}$$

where Q_t = the Li adsorption capacity at time t (mg/g)
Q_e = the Li adsorption capacity at equilibrium (mg/g)
t = the adsorption time (h)
k = the adsorption rate constant (g/mg·h)

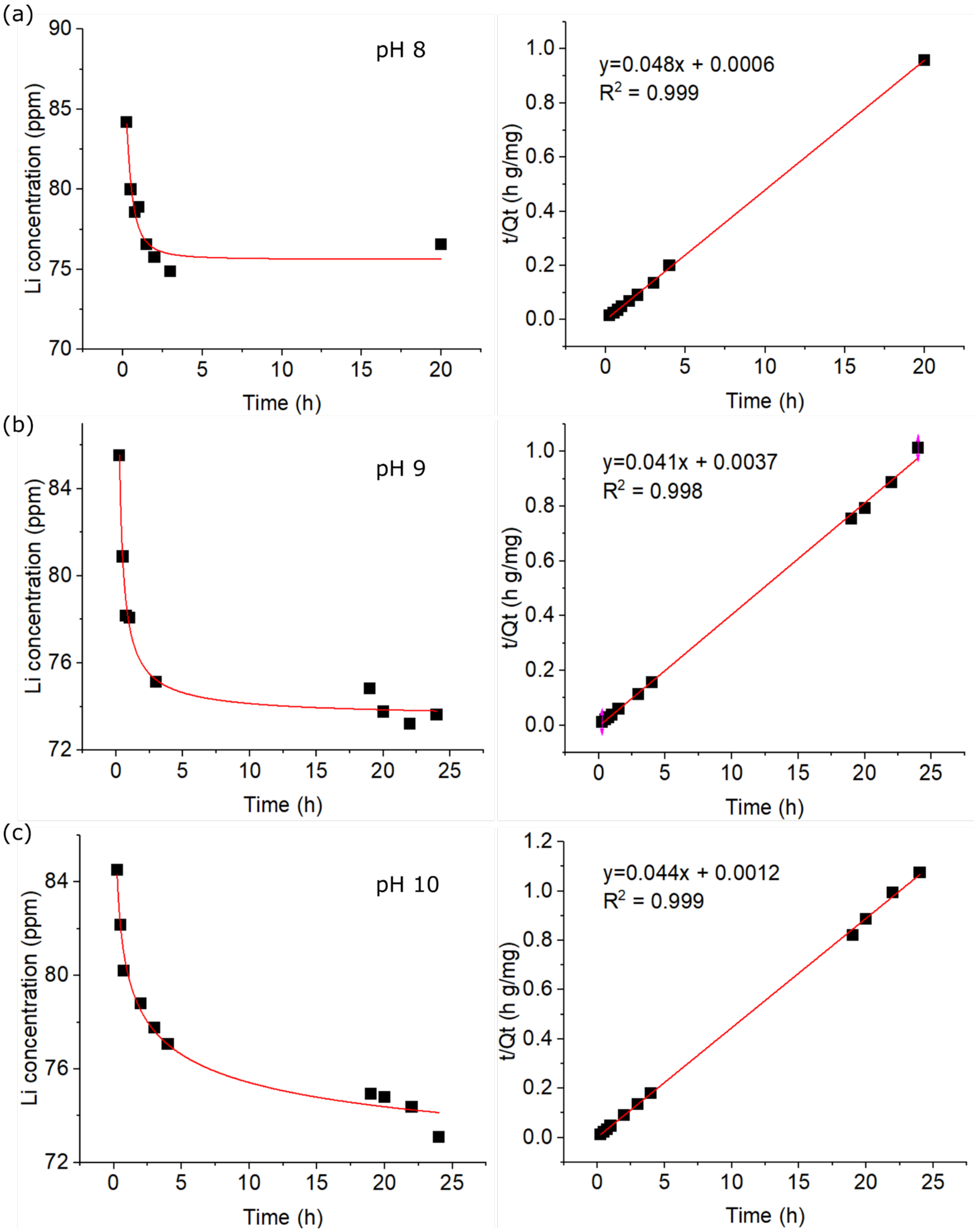

Figure 5. Adsorption kinetics of HMnO (left) and pseudo-second-order kinetics results (right) at (a) pH 8, (b) pH 9, and (c) pH 10

Table 1 summarizes the model parameters and the correlation coefficients (R^2). The R^2 values for the pseudo-second-order kinetics model at different pH levels were above 0.99 and the Q_e values calculated by the model ($Q_{e,model}$) were very close to the experimental values ($Q_{e,exp}$). The k values were calculated to be 0.384, 0.449, and 1.646 g/mg·h at pH levels of 8, 9, and 10, respectively. The results show that the pseudo-second-order kinetics model is suitable for describing the Li adsorption onto HMnO and the adsorption process is chemisorption (Li-H exchange). The reaction in this process is as follows:

$$\mathrm{HMnO} + \mathrm{Li}^+ \rightarrow \mathrm{LMnO} + \mathrm{H} \tag{5}$$

Table 1. Kinetic parameters of Li adsorption in brines at different pH levels

Brine alkalinity	R^2	k (g/mg·h)	$Q_{e,model}$ (mg/g)	$Q_{e,exp}$ (mg/g)
pH 8	0.999	0.384	20.83	21.8
pH 9	0.998	0.449	24.51	25.8
pH 10	0.999	1.646	22.5	22.5

The effect of the coexisting cations on the Li adsorption was studied in seven brines that contained multiple coexisting cations such as Li, sodium (Na), and potassium (K) as well as counterions at room temperature (Table 2). The Li adsorption capacities of HMnO in three synthetic brines were 19.9 mg/g, 19.2 mg/g, and 25.5 mg/g at pH 8, pH 9, and pH 10, respectively (Figure 6a). Moreover, the Li adsorption capacities in natural brines from geothermal systems at Teels Marsh, Nevada; British Columbia, and Hudson Ranch, California, were 22.7 mg/g, 24.6 mg/g, and 17.7 mg/g, respectively. The results indicate that the Li adsorption performance of HMnO was not affected by the presence of other coexisting cations in the brines, and the HMnO can be directly applied to highly saline and natural brines. Significant reduction in Li capacity was observed in brine from California's Salton Sea, where pH is 1.5, indicating that Li uptake does not work in acidic conditions, as we expected from the Li exchange experiment in HCl solution.

Table 2. Compositions and adsorptive capacities of brines with multiple coexisting cations

	Li (ppm)	Na (ppm)	K (ppm)	Counteranion	pH	Q_e (mg/g)
Synthetic brine pH 8	100	100	100	CO_3	8.0	19.9
Synthetic brine pH 9	100	100	100	CO_3	9.0	19.2
Synthetic brine pH 10	100	100	100	CO_3	10.0	25.5
Teels Marsh brine	73	37,720	2,308	Cl	9.62	22.7
British Columbia brine	811	112,200	7,705	Cl	6.95	24.6
Hudson Ranch brine	390	58,950	19,350	Cl	5.72	17.7
Salton Sea brine	340	63,350	28,650	Cl	1.51	Low

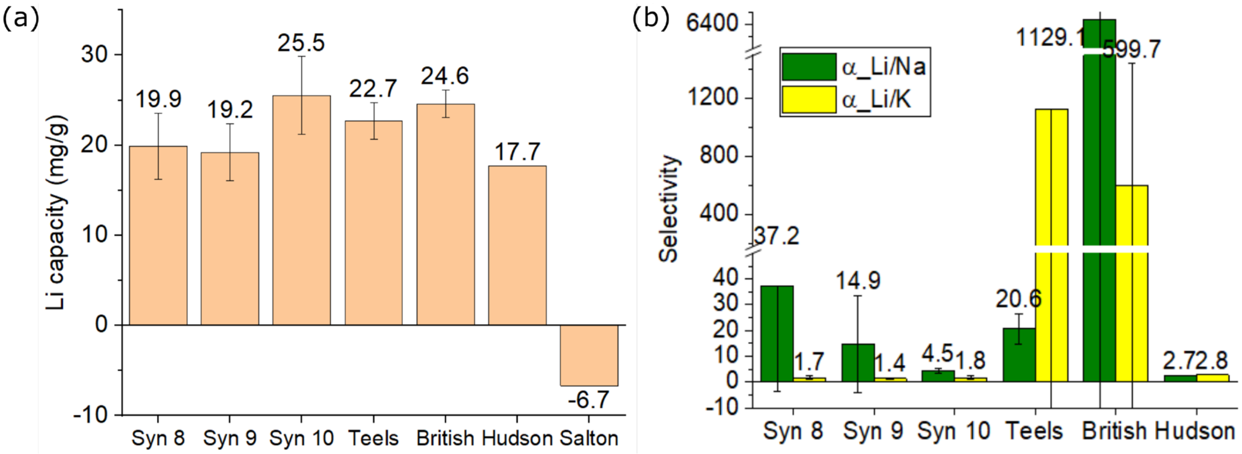

Figure 6. (a) Li adsorption capacity of HMnO and (b) Li over Na and K selectivities of HMnO in synthetic and natural brines

The adsorption performance of the HMnO in the brines (Table 2 except Salton Sea) was further studied in terms of the distribution coefficient (K_d) and selectivity (α), expressed as shown in Equations (6) and (7), respectively:

$$K_d = \frac{(C_{M,0} - C_M)}{C_M \times m_{HMnO}} \times V \tag{6}$$

$$\alpha = \frac{K_d^{Li}}{K_d^{M}} \tag{7}$$

A larger K_d indicates more adsorption of the cation in HMnO and therefore a larger α indicates preferable adsorption of Li over the coexisting metal cation (M) in the brines. As shown in Figure 6b, the α values for Li/Na (K_d^{Li}/K_d^{Na}) and Li/K (K_d^{Li}/K_d^{K}) are greater than 1 in all brines tested, suggesting that HMnO selectively adsorbs Li in brines with multiple coexisting cations.

Cycling performance of the HMnO was evaluated by repeating Li adsorption in the brines (Table 2 except Hudson Ranch and Salton Sea) and Li desorption. For the Li desorption experiment, Li-loaded HMnO was immersed in 0.1 M HCl containing 1000 ppm Mn overnight and then HMnO was regenerated. The Li adsorption capacity of the regenerated HMnO was retained after three cycles of adsorption and desorption (Figure 7a). Averaged Li capacities were 20.7 ± 4.4 mg/g, 19.1 ± 3.1 mg/g, and 22.6 ± 1.3 mg/g in synthetic brines at pH 8, 9, and 10, respectively, and 22.7 ± 2.1 mg/g and 24.6 ± 1.5 mg/g in Teels Marsh and British Columbia brines, respectively. The selectivity of HMnO for Li/Na varied greatly among cycle sets (Figure 7b). This may be due to inconsistent Na adsorption by HMnO in the natural brines, where Na concentration is 140–500 times higher than that of Li. Our understanding of Na-adsorption behavior by HMnO in natural brines would benefit from further investigation.

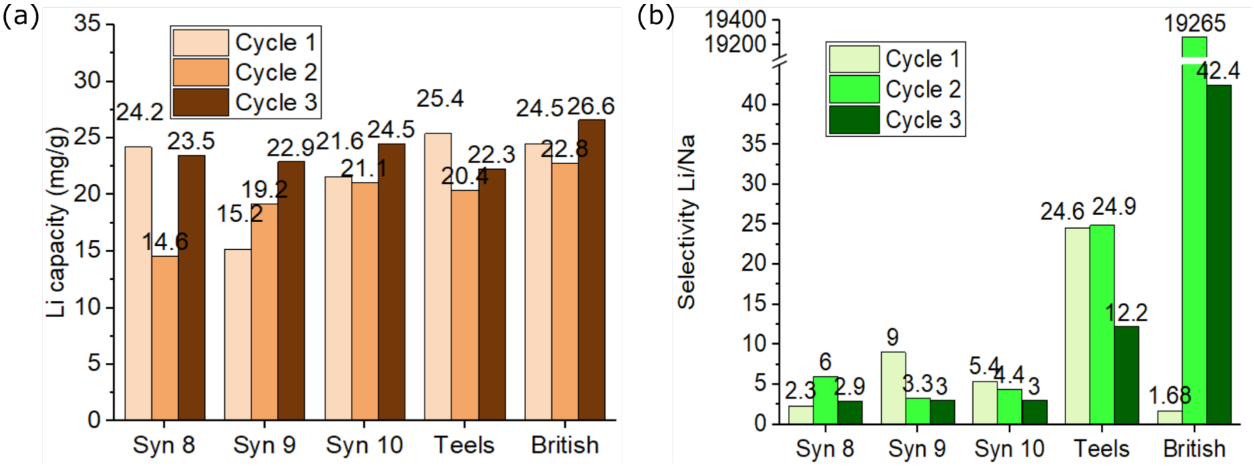

Figure 7. Cycling performance of HMnO in synthetic and natural brines: (a) Li adsorption capacity and (b) selectivity for Li/Na

Table 3. Cycling performance of HMnO in test brines

Brine	Average Li capacity over three cycles (mg/g)
Synthetic brine pH 8	20.7 ± 4.4
Synthetic brine pH 9	9.1 ± 3.1
Synthetic brine pH 10	22.6 ± 1.3
Teels Marsh brine	22.7 ± 2.1
British Columbia brine	24.6 ± 1.5

2.3 Comparison with Titanium-Based Ion-Sieves

To compare the adsorption performance of HMnO with those of other ion-sieves, hydrogen titanium oxides (HTOs) were synthesized according to a method reported in the literature (Chitrakar et al. 2014) and their adsorption performance in the brines (Table 2) was tested under identical experimental conditions. The Li adsorption capacities of HTO were 27.5 mg/g, 23.7 mg/g, and 20.6 mg/g in synthetic brines at pH 8, 9, and 10, respectively, and 18.1 mg/g, 40.3 mg/g, 18.8 mg/g in Teels Marsh, British Columbia, and Hudson Ranch brines, respectively, as listed in Table 4 and plotted in Figure 8a. As with results for HMnO, Li uptake by HTO in Salton Sea brine was significantly low (1.9 mg/mL). The selectivity of HTO for Li/Na was near 100 in simulated basic brines (pH 9 and pH 10), whereas selectivity in natural Teels Marsh brine (pH 9.6) was only 12 (Figure 8b). Further investigation of cycling performance and reproducibility for HTO is needed.

Table 4. Li adsorption capacities of HTOs in test brines

Brine	Li adsorption capacity (mg/g)
Synthetic brine pH 8	27.5
Synthetic brine pH 9	23.7
Synthetic brine pH 10	20.6
Teels Marsh brine	18.1
British Columbia brine	40.3
Hudson Ranch brine	18.8

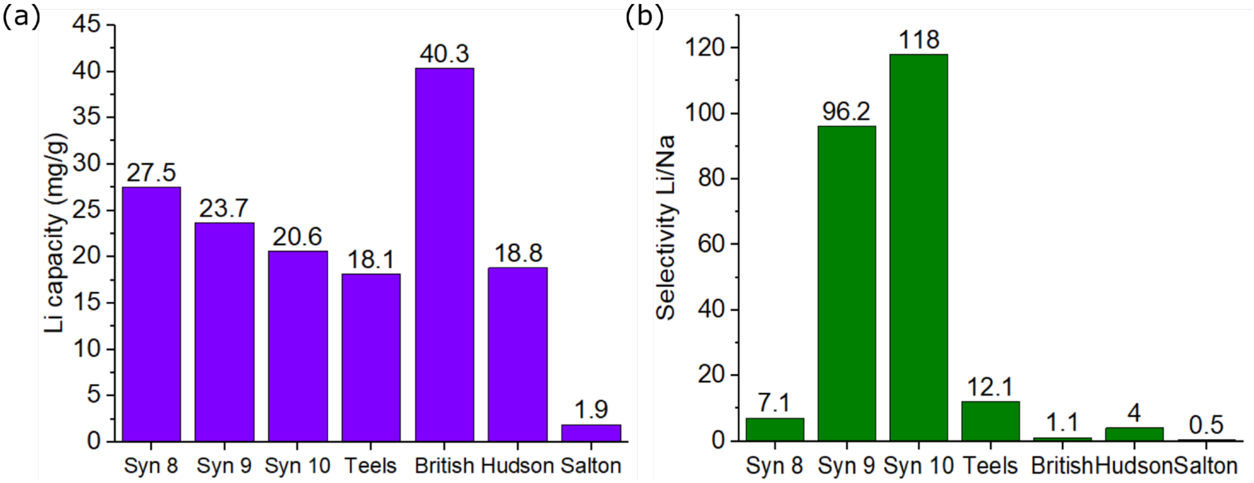

Figure 8. (a) Li adsorption capacity of HTO and (b) selectivity of HTO for Li/Na in brines

The adsorption performance comparison of HMnO and HTO was further investigated in brines where Li concentration varied from 7 ppm–5,600 ppm at a Li:Na molar ratio of 0.008–800 with different counterions (CO_3^{2-}, ClO_4^-, or Cl^-) at room temperature (Table 5). The concentration of HMnO or HTO in the brines was 1 mg/mL. As is shown for region (1) (Li/Na molar ratio >1) in Figure 9a-c, the Li adsorption capacity of HMnO increased with increasing Li concentration regardless of the type of counterions used. The same trend was observed with HTO. The maximum Li capacity reached 223 mg/g in the brine that had 5,600 ppm Li in the presence of ClO_4 anion. At constant Li concentration but varying Na concentration (Region [2] [Li/Na molar ratio <1] in Figure 9a-c), Li adsorption capacity of HMnO was not significantly affected by the concentration of coexisting Na cations, which is consistent with the above mentioned results of multiple coexisting cations. However, the average Li adsorption capacity (28 ± 6 mg/g) of HMnO in the presence of CO_3^{2-} ions was higher than those with ClO_4^- anions (11 ± 14 mg/g) and Cl^- ions (10 ± 7 mg/g). The same trend was observed with HTO. The results indicate that Li uptake by the HMnO and HTO is more efficient in basic conditions than in acidic conditions.

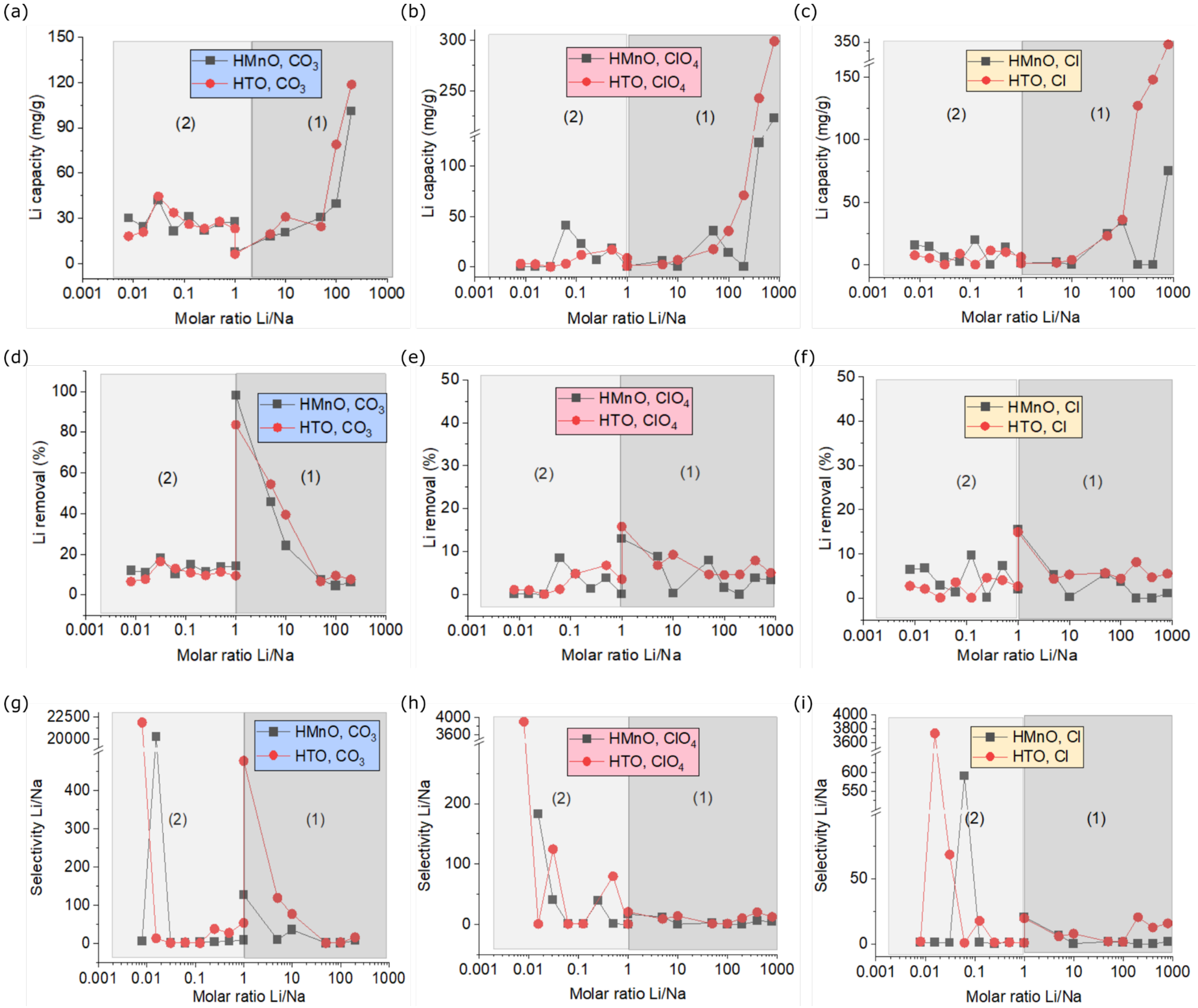

Figure 9. Top row: Li adsorption capacities of HMnO and HTO with counteranions (a) CO_3, (b) ClO_4, and (c) Cl. Middle row: Li removal percentages of HMnO and HTO with counteranions (d) CO_3, (e) ClO_4, and (f) Cl. Bottom row: Selectivities of HMnO and HTO for Li/Na with counteranions (g) CO_3, (h) ClO_4, and (i) Cl

Figure 9d-f shows Li removal percentages of the HMnO and HTO, calculated as shown in Equation (8). The Li removal by HMnO was almost complete (98%) from brines where the Li concentration was 7 ppm in the presence of CO_3, whereas only 13–16% of the Li was removed when the counteranion was ClO_4 or Cl (Figure 9d-f). HMnO removed a higher percentage of Li (98%) than HTO (82%) under identical conditions.

$$Li\ removal\ (\%) = \frac{(C_{Li,0} - C_{Li})}{C_{Li,0}} \times 100 \tag{8}$$

Figure 9g-i illustrates selectivities of HMnO and HTO for Li/Na. In Region (1), the selectivity of HMnO decreased with increasing Li concentration regardless of which counteranion was used. The maximum selectivity of HMnO was 127 at 7 ppm Li in the presence of CO_3 anions, while selectivities with ClO_4 and Cl anions were 17 and 21, respectively. For comparison, the maximum selectivity of HTO was 477 at 7 ppm Li in the presence of CO_3, and the selectivity decreased with increasing Li concentration. When ClO_4 or Cl was used as counteranion, the selectivity of HTO decreased and then slightly increased with increasing Li concentration. At constant Li concentration in region (2), selectivities of both HMnO and HTO increased with increasing Na concentration, but the variation is huge. Fundamental understanding is needed to explain the large variation.

Table 5. Compositions of brines with various Li concentrations and counteranions

	Li (ppm)	Na (ppm)	Molar ratio Li	pH of brines with different counteranions		
				CO_3	ClO_4	Cl
Region (1)	7	23	1	10.1	8.3	7.4
	35	23	5	10.5	7.3	6.6
	70	23	10	10.8	6.9	6.1
	350	23	50	11.2	6.3	5.6
	700	23	100	11.3	6.1	5.3
	1,400	23	200	11.5	5.9	5.5
	2,800	23	400	N/A	5.7	5.4
	5,600	23	800	N/A	5.7	5.6
Region (2)	174	575	1	11.0	6.0	5.8
	174	1,150	0.5	10.9	5.8	6.0
	174	2,300	0.25	10.9	5.7	5.7
	174	4,600	0.125	10.8	5.6	5.8
	174	9,200	0.062	10.7	5.6	5.7
	174	18,400	0.031	10.7	5.7	5.9
	174	36,800	0.015	10.5	5.9	5.8
	174	73,600	0.008	10.5	6.0	5.5

3.0 Core/Shell Magnetic Nanoparticles

3.1 Synthesis of Core/Shell Magnetic Nanoparticles

For the magnetic cores, Fe_3O_4 particles were synthesized by mixing ferric chloride with sodium acetate in ethylene glycol (Deng et al. 2005). The solution was placed in a Teflon-lined stainless steel autoclave and heated at 200°C for 18 h. After the particles were recovered through filtration, the powder was washed with ethanol and then dried at 60°C. The morphology and size of the Fe_3O_4 particles were examined by transmission electron microscopy (TEM) (Figure 10a). The pristine particles were spherical and had a mean diameter of 645 ± 200 nm. The PXRD pattern of the particles (Figure 10c) shows diffraction peaks with 2θ at 18.4°, 30.1°, 35.7°, 37.2°, 43.3°, 53.9°, 57.5°, and 63.0° which can be indexed to the (111), (220), (311), (222), (400), (422), (511), and (440) of Fe_3O_4, respectively. For better adhesion of the HMnO shell to the surface of the Fe_3O_4 core, the Fe_3O_4 particles were functionalized with hydrophilic carbon shells by a hydrothermal carbonization of glucose (Li et al. 2008). The resulting Fe_3O_4@C (F@C) nanoparticles were covered with a uniform carbon layer 15.7 ± 5 nm thick (Figure 10b) and showed a PXRD pattern identical to that of the Fe_3O_4 core (Figure 10c). The Fe_3O_4 and F@C were further characterized by magnetic saturation experiments to assess their intrinsic magnetic properties. Room-temperature vibrating-sample magnetometry measurements showed that saturation magnetizations of Fe_3O_4 and F@C were 71 emu/g and 37.8 emu/g, respectively (Figure 10d). The reduction in saturation magnetization after carbon coating may be attributed to partial oxidation of the Fe in the Fe_3O_4 core during the coating process.

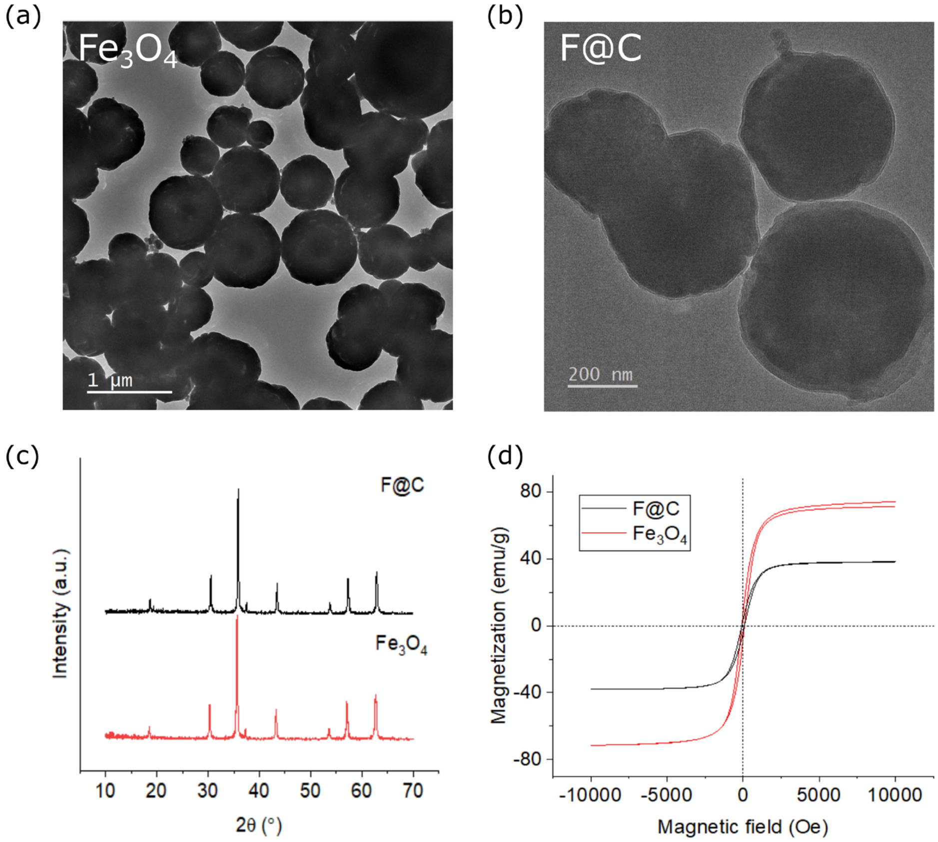

Figure 10. TEM images of (a) Fe_3O_4 and (b) F@C. (c) PXRD patterns and (d) magnetic saturation of Fe_3O_4 and F@C

To coat the magnetic cores with HMnO shells, a MnO_2 layer was grown on the as-synthesized Fe_3O_4 or F@C nanoparticles by a hydrothermal reaction; then the MnO2 was converted to LMnO and then HMnO, resulting in the formation of F@HMnO and F@C@HMnO core/shell structures. The TEM image of HMnO presented in Figure 11a shows nanorods that averaged 52 ± 24 nm in diameter and 580 ± 64 nm long. According to the TEM images (Figure 11b and c), F@LMnO and F@C@LMnO exhibit perfect core/shell structures; the LMnO shell thicknesses are 218 ± 36 nm for F@LMnO and 345 ± 78 nm for F@C@LMnO. The PXRD patterns of the F@HMnO and F@C@HMnO (Figure 11d) show diffraction peaks characteristic of both Fe_3O_4 and HMnO, indicating coexistence of Fe_3O_4 and HMnO in the core/shell nanoparticles. According to elemental analysis of the core/shell structures, the masses of the HMnO shells are estimated to be 78.8% within F@HMnO and 78.8% within F@C@HMnO. The F@HMnO and F@C@HMnO core/shell powders aggregated very quickly when an external magnetic field was applied, indicating excellent magnetic responsiveness of the core/shell structures (Figure 11e and f). Measurement of saturation magnetization of the core/shell structures is currently underway.

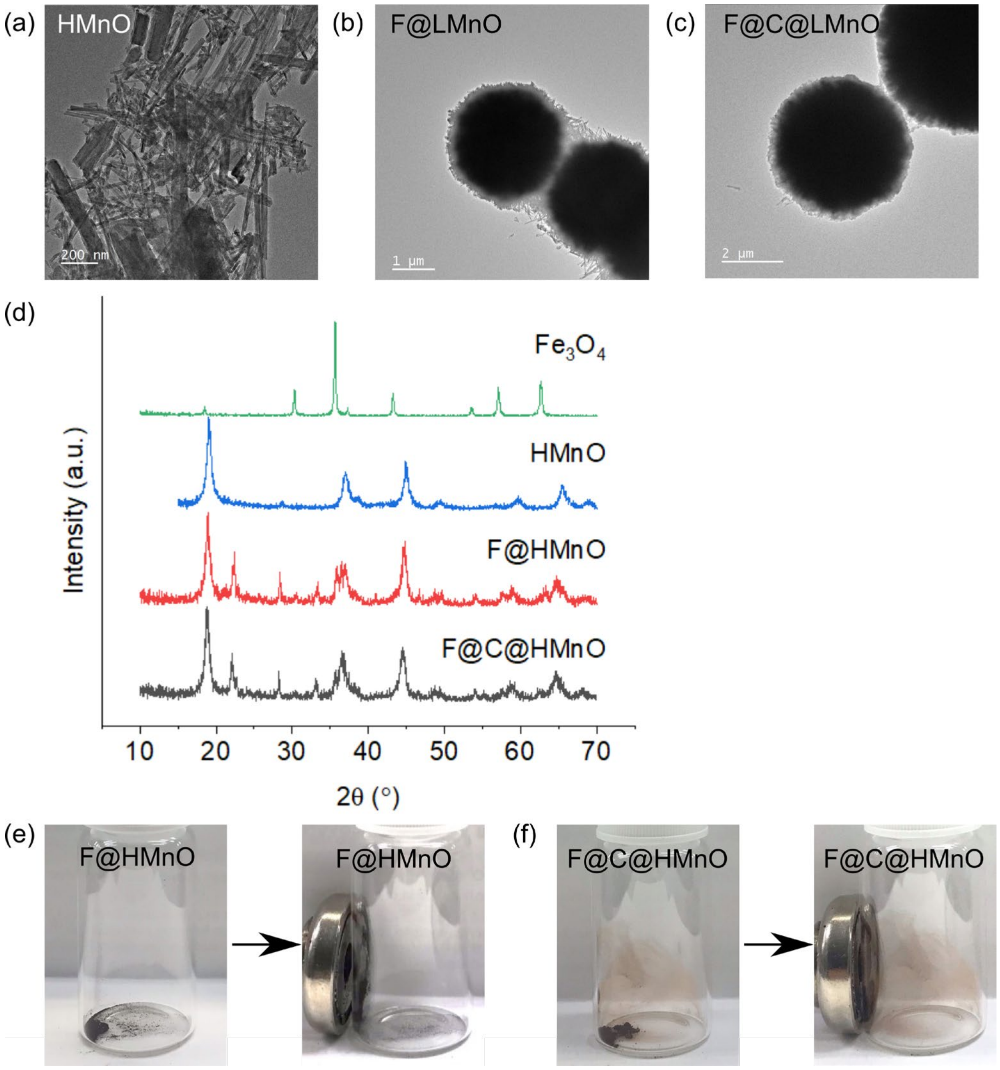

Figure 11. TEM images of (a) HMnO, (b) F@LMnO, and (c) F@C@LMnO. (d) PXRD patterns of Fe_3O_4, HMnO, F@HMnO, and F@C@HMnO. Digital pictures of (e) F@HMnO and (f) F@C@HMnO powder without and with permanent magnet adjacent

3.2 Lithium Extraction from Brines by Core/Shell Particles

The adsorption performance of the F@HMnO and F@C@HMnO core/shell magnetic nanoparticles in the complex brines (Table 2, except Salton Sea) was studied. The concentration of F@HMnO or F@C@HMnO in each of the brines was 1.5 mg/mL. The Li adsorption capacities of F@HMnO in the synthetic brines were 8 mg/g, 10.1 mg/g, and 9.1 mg/g at pH 8, 9, and 10, respectively (Figure 12a). The Li adsorption capacities in the Teels Marsh, British Columbia, and Hudson Ranch brines were 9.8 mg/g, 0.13 mg/g, and 2.9 mg/g, respectively. The Li adsorption capacities of F@C@HMnO at the three pH levels were higher than those of F@HMnO: 12.3 mg/g, 13.5 mg/g, and 13.3 mg/g at pH 8, 9, and 10, respectively, in the synthetic brines and 12.5 mg/g, 15 mg/g, and 9.8 mg/g in the Teels Marsh, British Columbia, and Hudson Ranch brines, respectively. This result indicates that both types of core/shell magnetic nanoparticles exhibit good Li adsorption behavior. The Li capacities of the core/shell structures are lower than that of pristine HMnO (Figure 5a) because given the same mass of sorbent, the core/shell structures include the Fe_3O_4 core, which has much lower Li capacity than HMnO.

Table 6. Li adsorption capacities of F@HMnO and F@C@HMnO in synthetic and natural brines

Brine	Li adsorption capacity (mg/g)	
	F@HMnO	F@C@HMnO
Synthetic brine pH 8	8	12.3
Synthetic brine pH 9	10.1	13.5
Synthetic brine pH 10	9.1	13.3
Teels Marsh brine	9.8	12.5
British Columbia brine	0.13	15.0
Hudson Ranch brine	2.9	9.8

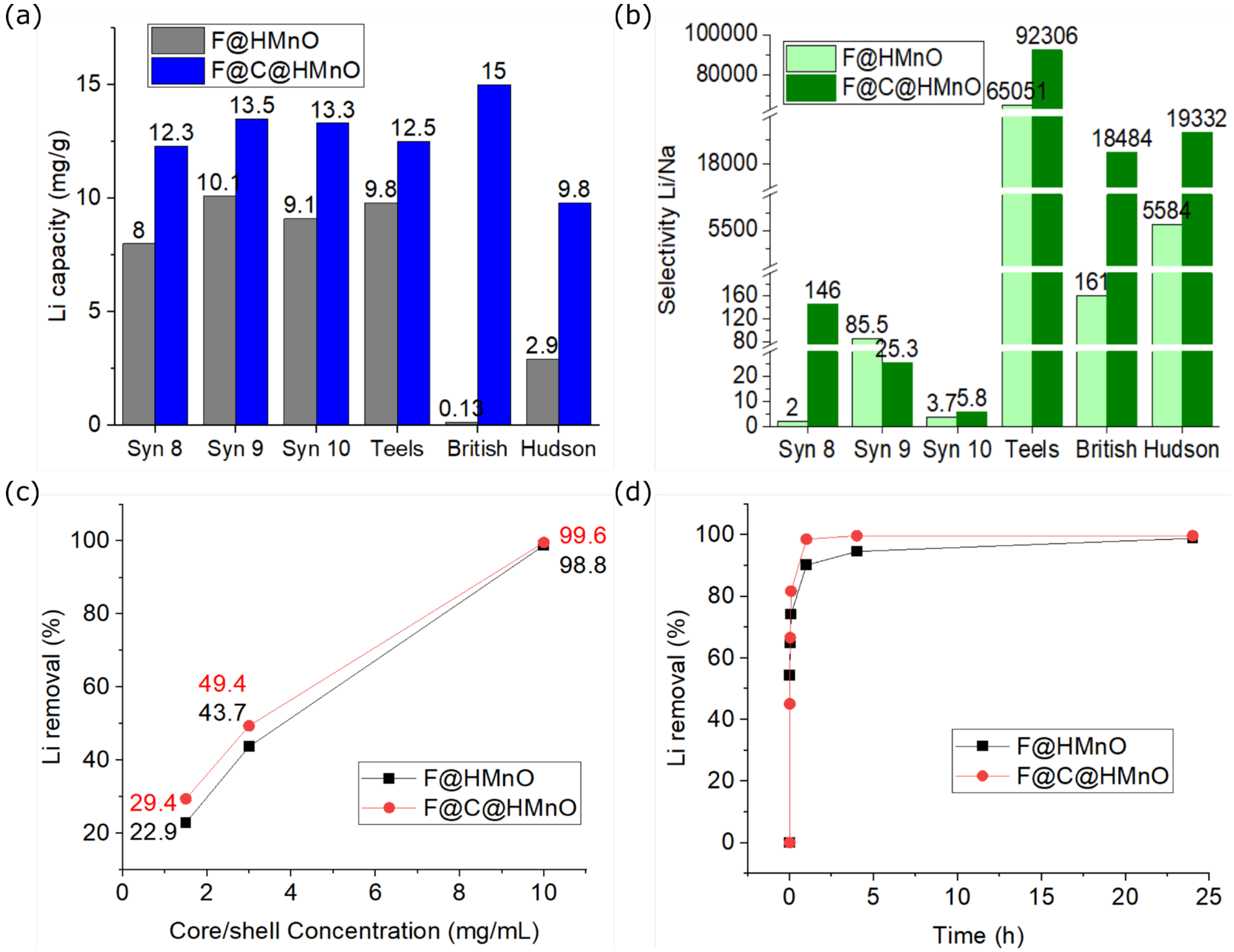

Figure 12. (a) Li adsorption capacities of F@HMnO and F@C@HMnO, (b) selectivity of F@HMnO and F@C@HMnO for Li/Na, (c) Li removal percentage as a function of core/shell magnetic nanoparticle concentration in Teels Marsh brine, and (d) Li removal percentage as a function of time at a concentration of 10.0 mg/mL in Teels Marsh brine

As we already observed from HMnO, selectivity of the F@HMnO and F@C@HMnO for Li/Na varies widely (Figure 12b). Adsorption of Na in natural brines was negligible, resulting in extremely large selectivity for Li/Na. Further investigation of Na adsorption by the core/shell magnetic nanoparticles and cycling performance is ongoing.

The Li removal percentage was studied as a function of core/shell magnetic nanoparticle concentrations (Figure 12c). As the concentration of F@HMnO in Teels Marsh brine increased from 1.5 mg/mL to 3 mg/mL and 10 mg/mL, Li removal percentage increased from 22.9% to 43.7% and 98.8%. Similarly, Li removal percentage by F@C@HMnO in Teels Marsh brine increased from 29.4% to 49.4% and 99.6% at the same three nanoparticle concentrations. As shown in Figure 12d, at 10 mg/mL in Teels Marsh brine, a significant amount of Li was removed after only 5 min incubation (74.2% by F@HMnO and 81.7% by F@HMnO) and Li removal percentages above 90% were achieved within 1 h incubation (90.1% by F@HMnO and 98.5% by F@C@HMnO).

3.3 Magnetic Response of Core/Shell Colloidal Solution

Magnetic response of a colloidal core/shell particle solution was tested using permanent magnets. F@C@HMnO was dispersed in Teels Marsh brine (Table 2) at a concentration of 1.5 mg/mL (Figure 13a). When a weak permanent magnet (1 cm × 1 cm, surface field unknown) was placed next to the solution container for 1 min, some F@C@HMnO was collected from the brine but some F@C@HMnO remained in the solution or precipitated to the bottom of the container (Figure 13b). With a strong permanent magnet (2.5 cm × 2.5 cm size, surface field 6,350 G), nearly all the F@C@HMnO was collected from the brine within 1 min, indicating that F@C@HMnO can be effectively separated from aqueous solution with a strong magnetic field (Figure 13c). Systematic investigation on the retention rate of the core/shell magnetic nanoparticles from the aqueous solution will be performed at different magnetic field strengths to determine optimal magnetic strength for magnetic test loop evaluation.

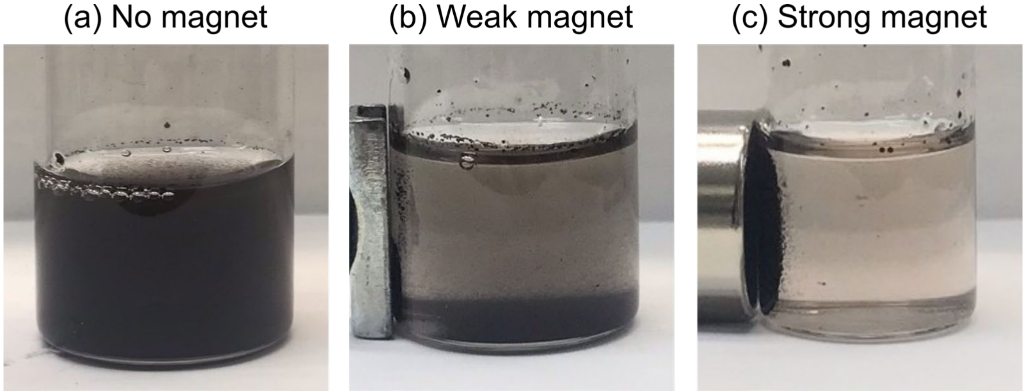

Figure 13. Photographs of F@C@HMnO colloidal solution (a) without magnet, (b) beside a weak permanent magnet, and (c) beside a strong permanent magnet

4.0 Conclusion and Next Steps

The PNNL team successfully developed core/shell magnetic nanoparticles that are composed of Li ion-sieve shells on magnetic cores for selective Li uptake from brines. Though the initial results are very promising, further work is needed to improve Li uptake properties of the core/shell magnetic nanoparticles, including optimizing synthetic conditions of core shell particle size, magnetic saturation, shell thickness, and the polymer coating. Also, the automated adsorption/desorption cycling system needs to be improved to continuously feed solutions of brine, sorbent, and stripping agent and to separate sorbents using magnetic fields.

5.0 References

Chitrakar, R., Y. Makita, K. Ooi, and A. Sonoda. 2014. “Lithium recovery from salt lake brine by H_2TiO_3.” *Dalton Transactions* 43 (23): 8933-8939. https://doi.org/10.1039/C4DT00467A.

Deng, H., X. Li, Q. Peng, X. Wang, J. Chen, and Y. Li. 2005. “Monodisperse Magnetic Single-Crystal Ferrite Microspheres.” *Angewandte Chemie International Edition* 44 (18): 2782-2785. https://doi.org/10.1002/anie.200462551.

Elsaidi, S. K., M. A. Sinnwell, A. Devaraj, T. C. Droubay, Z. Nie, V. Murugesan, B. P. McGrail, and P. K. Thallapally. 2018. “Extraction of rare earth elements using magnetite@MOF composites.” *Journal of Materials Chemistry A* 6 (38): 18438-18443. https://doi.org/10.1039/C8TA04750B.

Kumar, A., H. Fukuda, T. A. Hatton, and J. H. V. Lienhard. 2019. “Lithium Recovery from Oil and Gas Produced Water: A Need for a Growing Energy Industry.” *ACS Energy Letters* 4 (6): 1471-1474. https://doi.org/10.1021/acsenergylett.9b00779.

Li, Y., J. Wu, D. Qi, X. Xu, C. Deng, P. Yang, and X. Zhang. 2008. “Novel approach for the synthesis of Fe_3O_4@TiO_2 core–shell microspheres and their application to the highly specific capture of phosphopeptides for MALDI-TOF MS analysis.” *Chemical Communications* (5): 564-566. https://doi.org/10.1039/B716055K.

Liu, J., P. F. Martin, and B. P. McGrail. 2021. “Rare-earth element extraction from geothermal brine using magnetic core-shell nanoparticles-techno-economic analysis.” *Geothermics* 89: 101938. https://doi.org/10.1016/j.geothermics.2020.101938.

Ünlü, N., and M. Ersoz. 2007. “Removal of heavy metal ions by using dithiocarbamated-sporopollenin.” *Separation and Purification Technology* 52 (3): 461-469. https://doi.org/10.1016/j.seppur.2006.05.026.

Wang, X., and Y. Li. 2003. “Synthesis and Formation Mechanism of Manganese Dioxide Nanowires/Nanorods.” *Chemistry – A European Journal* 9 (1): 300-306. https://doi.org/10.1002/chem.200390024.

Xu, X., Y. Chen, P. Wan, K. Gasem, K. Wang, T. He, H. Adidharma, and M. Fan. 2016. “Extraction of lithium with functionalized lithium ion-sieves.” *Progress in Materials Science* 84: 276-313. https://doi.org/10.1016/j.pmatsci.2016.09.004.

Zandevakili, S., M. Ranjbar, and M. Ehteshamzadeh. 2014. “Recovery of lithium from Urmia Lake by a nanostructure MnO_2 ion sieve.” *Hydrometallurgy* 149: 148-152. https://doi.org/10.1016/j.hydromet.2014.08.004.

Pacific Northwest National Laboratory

902 Battelle Boulevard
P.O. Box 999
Richland, WA 99354

1-888-375-PNNL (7665)

www.pnnl.gov